Role of Horizontal Advection of Seasonal-Mean Moisture in the Madden–Julian Oscillation: A Theoretical Model Analysis

FEI LIU

Earth System Modeling Center, and Climate Dynamics Research Center, Nanjing University of Information Science and Technology, Nanjing, China

BIN WANG

Department of Atmospheric Sciences, and Atmosphere–Ocean Research Center, University of Hawai'i at Mānoa, Honolulu, Hawaii

(Manuscript received 21 January 2016, in final form 23 May 2016)

ABSTRACT

The impact of horizontal advection of seasonal-mean moisture (SMM) on Madden–Julian oscillation (MJO) dynamics is investigated here using a theoretical model that includes moisture advection processes. The zonal advection of SMM with an eastward gradient is found to produce planetary-scale instability and promote slow eastward propagation corresponding to an intraseasonal periodicity. This is because the SMM advection by an anomalous easterly of the Kelvin waves generates a moisture source to the east of precipitation, which favors eastward propagation and unstable growth. On the other hand, the advection of SMM with a westward gradient results in a westward-propagating unstable mode. For a realistic SMM distribution, the simulated eastward propagation is enhanced over the Indo-Pacific warm pool, while the westward propagation prevails over the central-eastern Pacific. In contrast to the zonal advection of SMM, the meridional advection of SMM only affects short waves and leaves planetary waves nearly unaffected.

The effect of zonal advection of SMM suggests an important mechanism for explaining the eastward propagation and growth of the MJO over the Indo-Pacific warm pool when the SMM increases eastward. However, this mechanism alone produces unrealistic Kelvin wave–like structure and strong westward propagation in the central-eastern Pacific; both disagree with observations. These caveats, however, can be remitted if the planetary boundary layer (PBL) moisture convergence feedback is included, which couples the Kelvin wave and the Rossby wave via precipitation heating, producing a realistic horizontal structure and also substantially suppressing the unrealistically growing, westward-propagating mode in the central-eastern Pacific.

1. Introduction

The Madden–Julian oscillation (MJO), named after its discoverers (Madden and Julian 1971, 1972, 1994), is the most energetic intraseasonal oscillation in the tropical atmosphere. The MJO is usually characterized by a slowly eastward-propagating (about $5\,m\,s^{-1}$), planetary-scale baroclinic circulation cell, and its convection center usually prevails over the Indo-Pacific warm pool (Knutson and Weickmann 1987; Wang and Rui 1990; Hendon and Salby 1994; Maloney and Hartmann 1998; Kiladis et al. 2005; Zhang 2005). We present an important mechanism to explain MJO development, propagation, and scale selection in this paper.

Owing to considerable interest in understanding the underlying cause of the MJO, a number of theories have been proposed, such as wave–convective instability of the second kind (wave-CISK; Lau and Peng 1987), evaporation–wind feedback (Emanuel 1987; Neelin et al. 1987; Wang 1988b), planetary boundary layer (PBL) moisture convergence feedback and frictionally coupled Kelvin–Rossby wave theory (Wang 1988a; Li

Earth System Modeling Center Contribution Number 114.

Corresponding author address: Dr. Fei Liu, Earth System Modeling Center, Nanjing University of Information Science and Technology, 219 Ningliu Rd., Nanjing 210044, China.
E-mail: liuf@nuist.edu.cn

DOI: 10.1175/JCLI-D-16-0078.1

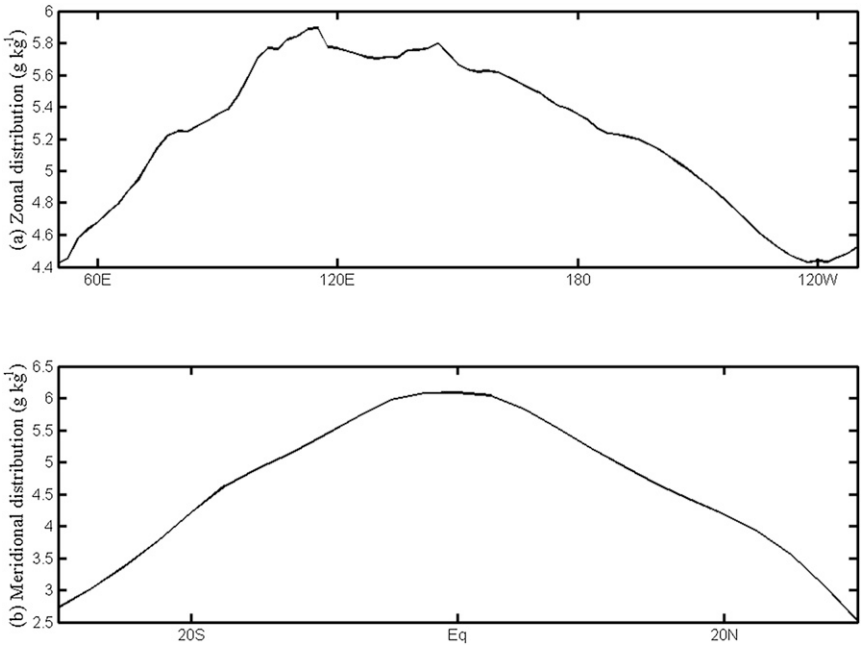

FIG. 1. Climatological distribution of SMM. (a) Zonal (10°S–10°N average) and (b) meridional (60°E–140°E average) distributions of climatological-mean (1948–2013), boreal-winter (November–March), lower-tropospheric (825–500 hPa) specific humidity.

and Zhou 2009; Liu and Wang 2012a), cloud–radiation feedback (Hu and Randall 1994; Raymond 2001; Fuchs and Raymond 2005; Andersen and Kuang 2012; Wang et al. 2013), convection–moisture feedback (Woolnough et al. 2001; Grabowski and Moncrieff 2004; Raymond and Fuchs 2009; Kuang 2011; Sobel and Maloney 2012, 2013), and multiscale interaction (Majda and Biello 2004; Majda and Stechmann 2009, 2011; Wang and Liu 2011; Liu and Wang 2012b, 2013).

In addition to the aforementioned mechanisms, recent general circulation model (GCM) experiments suggested that horizontal moisture advection is particularly important for MJO simulation (Maloney 2009; Maloney et al. 2010) and that correct simulation of seasonal-mean moisture (SMM) is important for MJO simulation (Kim et al. 2011; Benedict et al. 2014). Studies using observations noted the zonal advection of SMM is important for the MJO initiation and development over the Indian Ocean (Kiranmayi and Maloney 2011; Hsu and Li 2012; Zhao et al. 2013; Sobel et al. 2014). During the boreal winter from November to March, the MJO is intensified over the Maritime Continent when the eastward gradient of SMM anomalies exists because of the simultaneous positive sea surface temperature (SST) anomalies over the central Pacific (Liu et al. 2015). In the monthly mean NCEP–Department of Energy (DOE) AMIP-II reanalysis (Kanamitsu et al. 2002), the SMM is maximum over the warm pool region (Fig. 1); thus, the zonal gradient of SMM is eastward over the Indo-Pacific warm pool and westward over the central-eastern Pacific, and the zonal advection of SMM by lower-tropospheric easterly winds of the MJO would support MJO development over the Indian Ocean. We use the daily Advanced Very High Resolution Radiometer (AVHRR) outgoing longwave radiation (OLR) from the NOAA polar-orbiting satellites (Liebmann and Smith 1996) to represent the MJO convection and use the daily zonal wind and specific humidity from the NCEP–NCAR reanalysis (Kalnay et al. 1996) to represent the MJO circulation and moisture during 1979–2013. Figure 2 shows observed relations among MJO convection, moisture anomalies and zonal SMM advection. For the developing MJO over the Indian Ocean (Wheeler and Hendon 2004), the moisture anomalies of the MJO lead the convective center to the east. The positive zonal advection of SMM by the lower-tropospheric easterly winds leads MJO moisture anomalies to the east (Fig. 2a). This means the zonal advection of SMM tends to moisten the lower troposphere and enhance MJO convection. For the decaying MJO over the western Pacific, the zonal advection of SMM tends to dry the lower troposphere and suppress MJO convection (Fig. 2b). By considering an f plane, first baroclinic mode in the weak temperature gradient approximation, the meridional advection of SMM is found to destabilize the eastward propagation (Sobel et al. 2001), while the

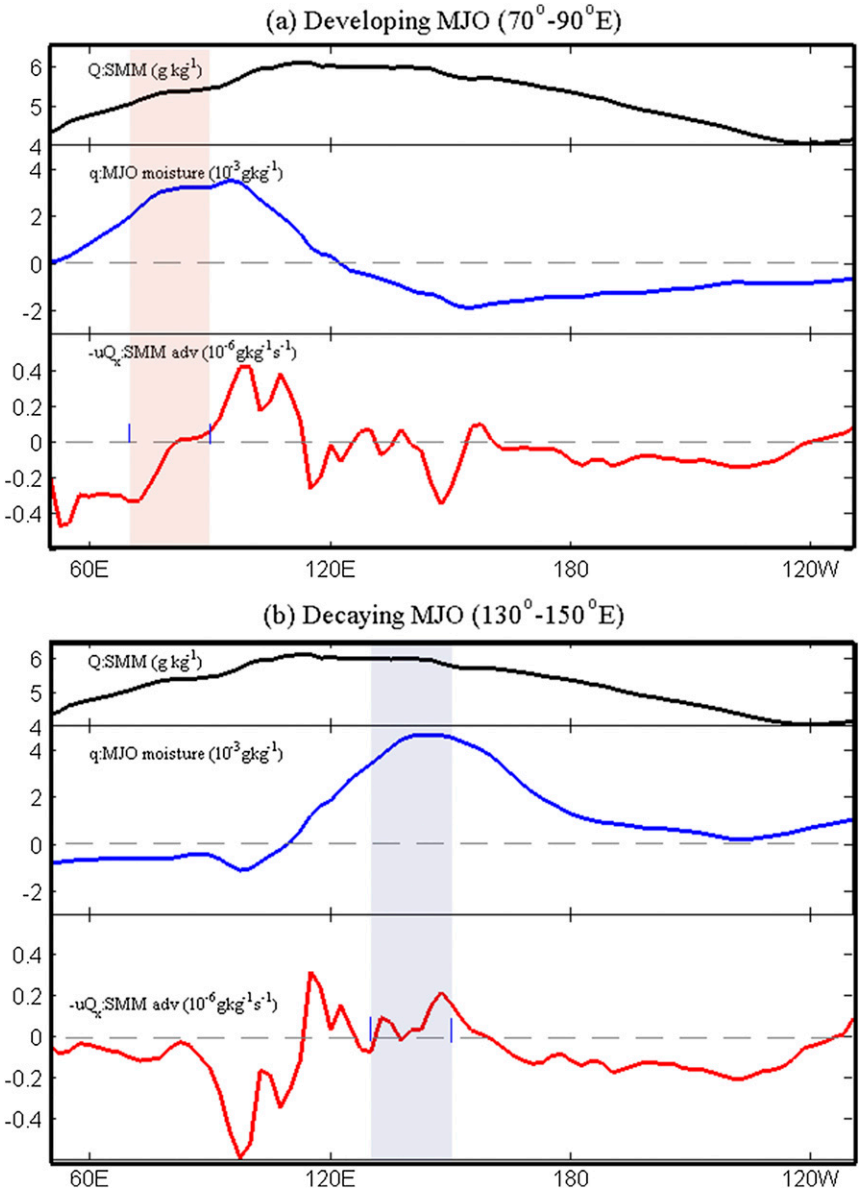

FIG. 2. Observed SMM advection. (a) The composite equatorial (10°S–10°N) averaged, lower-tropospheric (825–500 hPa), 20–80-day filtered moisture (blue) and zonal SMM advection (red) during the boreal winter (November–March) for the developing MJO for which the area (10°S–10°N, 70°–90°E) averaged 20–80-day filtered OLR is less than one negative standard deviation. The climatological-mean SMM (as in Fig. 1a) is also shown by the black curve. The shaded rectangle denotes the convective center. (b) As in (a), but that for the decaying MJO for which the area (10°S–10°N, 130°–150°E) averaged 20–80-day filtered OLR is less than one negative standard deviation.

meridional advection of SMM only simulates the neutral mode on a β plane (Sukhatme 2014). In view of these simulations, observations, and theoretical results, we aim to test the hypothesis that the horizontal advection of SMM is one of the important mechanisms for explaining MJO development, propagation, and scale selection.

The theoretical model used for testing the hypothesis is a modified version of the newly developed theoretical model for studying the essential dynamics of the MJO (Liu and Wang 2016). The model framework integrates the wave–convection interaction, the PBL frictional moisture convergence (FC) feedback and a simple convection–moisture feedback. The model extends the

Matsuno–Gill theory by incorporating moisture feedback to precipitation heating and a trio-interaction among low-frequency equatorial waves, boundary layer dynamics, and precipitation heating. Therefore, the model combines convectively coupled wave–PBL dynamics (Wang and Rui 1990; Wang and Li 1994; Kang et al. 2013) and a simple moisture process in the "moisture mode" (Raymond and Fuchs 2009; Sobel and Maloney 2013), whereas the complicated convection triggering process connected to the mean atmospheric moisture and the thermodynamics feedback of the moisture mode are not considered here. The model with the simplified Betts–Miller scheme can produce essential aspects of large-scale characteristics of the observed MJO: an equatorial planetary-scale, unstable system (over the Indo-Pacific warm pool) moving eastward slowly (resulting in an intraseasonal periodicity) with convectively coupled Kelvin–Rossby wave structure and rearward-tilted moisture and divergence anomalies. The model can also accommodate a variety of additional processes, providing a general framework for understanding MJO dynamics (Liu and Wang 2016). For this reason, we use it to test the aforementioned hypothesis.

To identify the potentially important role of basic-state moisture advection, we implement a moisture advection mechanism in the model. This improved model allows us to understand the mechanism by which SMM advection (by MJO circulation anomaly) affects the propagation, instability, and structure of the MJO. In this work, the simplified Betts–Miller scheme is used to incorporate moisture feedback. The model can be run with or without the PBL dynamics so that the impact of moisture advection can be examined in isolation or in combination with the PBL feedback.

In section 2, we introduce the theoretical model. In section 3, we show the properties of the linear normal modes affected by the uniform moisture advection process. In section 4, we present a few representative numerical solutions for realistic mean states. In section 5, we discuss the convection scheme. In section 6, we provide our conclusions.

2. Model framework

a. Basic equations

In the theoretical model, we parameterize large-scale precipitation heating based on a simplified Betts–Miller relaxation scheme (Betts 1986; Betts and Miller 1986; Frierson et al. 2004). For simplicity, we neglect momentum damping in the free troposphere and adopt the longwave approximation to filter out high-frequency waves. We choose a velocity scale of $C = 50\,\mathrm{m\,s^{-1}}$(the speed of the lowest internal gravity wave), a length scale of $\sqrt{C/\beta} = 1{,}500\,\mathrm{km}$ (the equatorial Rossby deformation radius), and a time scale of $\sqrt{1/C\beta} = 8.5\,\mathrm{h}$, where $\beta = 2.3\times10^{-11}\,\mathrm{m^{-1}\,s^{-1}}$ represents the leading-order curvature effect of Earth at the equator. The scales for geopotential and moisture anomalies are $C^2 = 2500\,\mathrm{m^2\,s^{-2}}$ and $4.8\,\mathrm{g\,kg^{-1}}$ (Wang 1988a), respectively. Thus, the nondimensional governing equations for the first baroclinic mode (Liu and Wang 2016) are the following:

$$\begin{aligned} u_t - yv &= -\phi_x,\\ yu &= -\phi_y,\\ \phi_t + u_x + v_y &= -P_r - \mu\phi,\\ q_t + Q(u_x + v_y) &= -P_r, \quad \text{and}\\ P_r &= \frac{1}{\tau}(q + \alpha\phi), \end{aligned} \tag{1}$$

where u and v are the zonal x and meridional y velocities, respectively, ϕ is the geopotential anomaly, and μ is the nondimensional Newtonian cooling coefficient. The parameter Q is the nondimensional vertical gradient of tropospheric background moisture, which is a function of prescribed SST (Wang 1988a). The term P_r is the precipitation associated with the diabatic heating of deep convection, which is parameterized by the simplified Betts–Miller scheme. In the precipitation equation, the first and second terms on the rhs indicate convection will relax moisture to its reference state counterpart and release the convective available potential energy (CAPE). Through this parameterization, the positive lower-tropospheric moisture anomalies and cold midtroposphere–warm boundary layer contrast both enhance precipitation. The term α is the coefficient of the reference moisture profile, measuring the relative contribution of environmental buoyancy to the CAPE parameterization. Positive α means the convection will release positive CAPE, and sensitivity experiments show that the model results are not sensitive to α. The term τ is the convective adjustment time, which measures how long it takes the convection to release CAPE and relax moisture back to its reference state (Neelin and Yu 1994). Here, we assume a slow adjustment; thus, $\tau = 12\,\mathrm{h}$ is in agreement with observations (Bretherton et al. 2004). Details of this model can be found in Liu and Wang (2016).

When the horizontal advection of SMM is added, the original moisture equation is replaced by

$$q_t + Q(u_x + v_y) + uQ_x + vQ_y = -P_r, \tag{2}$$

TABLE 1. Parameters and their default values used in the experiments. Adapted from Liu and Wang (2016).

Parameter	Description	Typical value used (nondimensional)
Q	Vertical SMM gradient between the lower (900–500 hPa) and upper (500–100 hPa) troposphere	0.9 [7.3 g kg^{-1}(400 hPa)$^{-1}$]
Q_b	Vertical SMM gradient at the top of the PBL (900 hPa)	1.6 [12.5 g kg^{-1}(100 hPa)$^{-1}$]
μ	Newtonian cooling coefficient	0.18 (6×10^{-6} s^{-1})
E	Ekman number in the PBL	1.1 (1/8 h)
d	PBL depth	0.25 (100 hPa)
α	Moisture reference coefficient	0.1
τ	Convective adjustment time	1.5 (12 h)

where Q_x and Q_y are the zonal and meridional gradients of SMM in the lower troposphere, respectively.

For comparison, the role of PBL moisture convergence is also included in the model. We use a well-mixed PBL model with the longwave approximation (Wang and Li 1994), in which the movement is driven by the pressure anomaly that is assumed to be equal to the pressure anomaly in the lower troposphere. Thus, the Ekman pumping w (Liu and Wang 2016) has the form of

$$w = d(d_1\phi_{yy} + d_2\phi_y), \tag{3}$$

where $d_1 = E/(E^2 + y^2)$, and $d_2 = -2Ey/(E^2 + y^2)^2$. The term d is the nondimensional PBL depth. The term E is the Ekman number in the PBL. The PBL moisture convergence acts to moisten the lower troposphere, and this process can be added in the moisture equation as follows:

$$q_t + Q(u_x + v_y) = -P_r + Q_b w, \tag{4}$$

where Q_b is the nondimensional effective background moisture in the PBL (i.e., the vertical gradient of the background moisture at the top of the boundary layer).

b. The theoretical model with both moisture advection and PBL processes

The model including both the moisture advection and PBL moisture convergence processes can be written as follows:

$$\begin{aligned} u_t - yv &= -\phi_x, \\ yu &= -\phi_y, \\ \phi_t + u_x + v_y - w &= -P_r - \mu\phi, \\ q_t + Q(u_x + v_y) + uQ_x + vQ_y &= -P_r + Q_b w, \\ P_r &= \frac{1}{\tau}(q + \alpha\phi), \quad \text{and} \\ w &= d(d_1\phi_{yy} + d_2\phi_y). \end{aligned} \tag{5}$$

The Ekman pumping is also added in the temperature equation because of continuity (Liu and Wang 2016). The original wave dynamics–moisture (WM) model can be obtained by neglecting these advection and PBL processes (i.e., by setting $Q_x = 0$, $Q_y = 0$, and $Q_b = 0$). Individual roles of zonal moisture advection, meridional moisture advection, and PBL moisture convergence can be investigated by only keeping a specific term in each test run. Standard values for the parameters used in this model are listed in Table 1.

c. Linear normal modes

To explore the role of horizontal advection of SMM, the zonally constant SMM gradient is investigated first. According to observations (Fig. 1), we choose the zonal gradient of SMM $Q_x = 0.06$, which represents a dimensional zonal gradient of 1.5 g kg^{-1} per 50° longitude, and the meridional gradient $Q_y = -0.24y\exp(-y^2/2)$, which represents a poleward meridional gradient of 3.5 g kg^{-1} per 30° latitude. Following previous works (Wang 1988a; Liu and Wang 2012a), the basic-state specific humidity is assumed to decrease exponentially from the surface upward, with an e-folding scale of 2.2 km. The surface specific humidity is estimated based on an empirical dependence on SST [i.e., $(0.972\text{SST} - 8.92) \times 10^{-3}$ kg kg^{-1}]. Thus, the SMM in the PBL (1000–900 hPa), lower troposphere (900–500 hPa), upper troposphere (500–100 hPa), and full troposphere (900–100 hPa) can be obtained, and the moisture vertical gradient at the top of the PBL Q_b can be calculated by the difference between the PBL and full troposphere, while the gradient in the troposphere Q can be calculated by the difference between the lower and upper troposphere.

To obtain the analytical solution, the zonally homogeneous background moisture is used, and the standard value over a warm SST of 29.5°C for the tropospheric vertical SMM gradient Q and the PBL moisture gradient Q_b are listed in Table 1. Thus, there is inconsistency between the zonally uniform SMM and zonal SMM gradient Q_x, which remains to be a good approximation and can be corrected in the numerical integration with a realistic distribution of background moisture.

Since the background moisture associated with SST is maximum in the tropics and decreases poleward over the Indo-Pacific warm pool during the boreal winter (Kang et al. 2013), we assume that the tropospheric zonal SMM gradient Q_x, the tropospheric vertical SMM gradient Q, and the PBL vertical moisture gradient Q_b all are maximum at the equator, having the values listed above and decreasing poleward with an e-folding damping scale of 30°.

For the zonally homogeneous SMM gradient, Eqs. (5) can be calculated by solving an eigenvalue problem. We assume that the solutions have a zonally propagating plane–wave structure in the form of $e^{i(kx-\omega t)}$; that is, the perturbations propagate at a real phase speed of $\mathrm{Re}(\omega)/k$ and with a linear growth rate of $\mathrm{Im}(\omega)$. Here, ω and k are frequency and wavenumber, respectively. After projecting Eqs. (5) onto the frequency–wavenumber domain, we can obtain a coefficient matrix for the five variables, and the eigenvalues and eigenvectors are calculated via matrix inversion. The Rossby and Kelvin waves, with their lowest meridional modes, can be studied using the first three meridional expansions of parabolic cylinder functions. Sensitivity experiments showed that higher meridional modes did not affect the results qualitatively.

A simple formula for the oscillation without the PBL and moisture advection can be obtained by considering the even simpler case of flow above the equator. In this case, Eqs. (5) are used, v and y are set to zero, and meridional derivatives are also ignored; thus, the dispersion equation can be simply written as follows:

$$\tau\sigma^3 + i\sigma^2 - \tau k^2\sigma - i(1-Q)k^2 = 0, \qquad (6)$$

which is a cubic equation when the moisture process is included.

Since the dispersion relation is determined by a cubic equation, the frequency has three solutions for each wavenumber. In this work, we only keep the positive frequency (i.e., $\omega > 0$), and the eastward (westward) propagation is selected by choosing positive (negative) wavenumber. In this work, we mainly focus on the eastward propagation, and the westward propagation will be discussed in the sensitivity experiments. The calculation also shows that one solution with positive frequency has a growth rate smaller than $-0.4\,\mathrm{day}^{-1}$, and we remove this unrealistic, strongly damped solution.

d. Numerical integration

To test the hypothesis that horizontal advection of SMM is important for the MJO, the realistic SMM, especially the realistic zonal variation of the SMM gradient, is studied by integrating the model from an initial value with linear heating over time. We solve this linear system numerically in a zonally periodic domain, and no fluxes of mass, momentum, and heat are applied at the meridional lateral boundary of 35°N and 35°S. The finite difference method is adopted in both time and space. The time integration scheme is forward differenced with a time step of 2.5 min. The spatial resolution is 2.5° by 2.5°. Sensitivity tests were performed using different spatial grid sizes, and the results showed no sensitivity to the horizontal resolution.

Simulations are initialized by the pressure perturbation with a Kelvin wave–like structure of $\phi = \phi_0 \sin(2\pi k_i x/L)$, where L is the nondimensional circumference of Earth at the equator, and k_i is the wavenumber of initial disturbances.

3. Idealized mean state

For simplicity, in this section we consider linear heating and the idealized SMM field. The idealized SMM distributions were described in section 2c. In the following analysis, we first focus on the effects of SMM advection on growth rate, propagation, and horizontal structure and then examine the combined effects of PBL frictional moisture feedback and SMM advection. This allows us to isolate the roles of SMM advection clearly.

a. Impact of SMM advection

Let us examine instability and periodicity (or propagation speed) first. Figure 3 shows the growth rate and frequency (periodicity) as a function of wavenumber for different moisture advection processes without the PBL feedback. Three cases are used for comparison. In the first case, only wave–moisture feedback under the Betts–Miller scheme is included, so it is without moisture advection. This case serves as a basic model, named the WM model for short. In the second and third cases, zonal Q_x and meridional Q_y moisture advections are added, respectively, so that the effects of moisture advection can be identified.

Without SMM advection, the Betts–Miller scheme only simulates a damped eastward-propagating mode, and short waves are strongly damped. The meridional advection of SMM mainly affects short waves, and the long waves are less affected. The growth rate of short waves is increased, though it remains negative. When an eastward SMM gradient is included, the SMM advection makes planetary-scale waves less damped, and wavenumber 1 becomes unstable; the short waves are strongly damped.

The frequency is changed significantly by the moisture advection processes (Fig. 3b). Without SMM advection, the WM-damped mode is nearly stationary, although

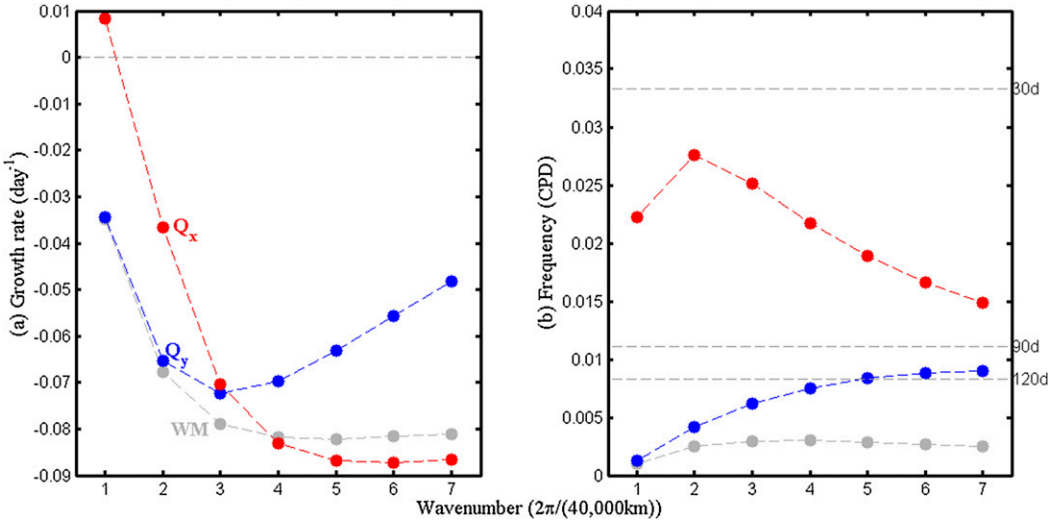

FIG. 3. Role of horizontal advection of SMM. (a) Growth rate (day^{-1}) and (b) frequency (cycles per day) as a function of wavenumber in the WM model (gray), the WM model with meridional SMM advection only (blue), and the WM model with zonal SMM advection only (red). The selection of these processes is given in section 2b.

still eastward, with a period longer than 120 days for all wavenumbers. The inclusion of the meridional advection tends to accelerate the eastward propagation of short waves, while the long waves are less affected. The eastward propagation is accelerated by the zonal SMM advection process for all wavenumbers, resulting in an oscillation of 30–90 days.

Since the MJO is viewed as coupled equatorial Kelvin and Rossby waves, it is worth analyzing how the horizontal moisture advection affects the horizontal structure of this coupled system, which can be shown by the eigenvector corresponding to each eigenvalue. Figure 4 shows the horizontal structure of the eastward-propagating wavenumber-1 mode. Without SMM advection (Fig. 4a), the WM mode exhibits that the equatorial low pressure anomalies are sandwiched by two off-equatorial high pressure gyres; the positive pressure anomalies, however, are in phase with the positive precipitation anomalies. This horizontal structure is unrealistic in the sense that 1) it is not a convectively coupled Kelvin–Rossby wave structure (or the Gill pattern) and 2) it has an erroneous relationship between precipitation and pressure anomalies. In the observations, precipitation is in quadrature with equatorial pressure anomalies; here, they are precisely in phase. When the zonal advection of SMM is included, the horizontal structure is drastically changed (Fig. 4b). The system is dominated by equatorial disturbances, and off-equatorial disturbances are almost completely suppressed. This horizontal structure is not a convectively coupled Kelvin–Rossby wave structure; rather, it looks like a Kelvin wave structure. The low pressure anomalies, in phase with the lower-tropospheric easterly wind anomalies, lead the positive precipitation center, while the positive pressure anomalies lag the convective center. The meridional moisture advection has an insignificant effect on the horizontal structure of wavenumber 1 (not shown).

Different from previous works (Sobel et al. 2001; Sukhatme 2014), we find that the meridional advection of SMM only affects short waves while keeping long waves unaffected. The zonal advection of SMM tends to provide an instability source for planetary waves, which results in an unstable wavenumber 1. The zonal moisture advection also plays a significant role in accelerating eastward propagation, resulting in a period on the intraseasonal time scale. However, the zonal moisture advection cannot couple the Kelvin and Rossby waves, resulting in a Kelvin wave–like mode.

b. *Effects of SMM advection in the presence of PBL dynamics*

What roles does the SMM advection play in the presence of PBL moisture convergence? Figure 5 shows the growth rate and frequency for different processes. We again use three cases for comparison. The first case has only the WM feedback, without the moisture advection and PBL feedback. The second case has the PBL feedback added ($Q_b > 0$). The third case has both the moisture advection and PBL moisture feedback added ($Q_x Q_y Q_b \neq 0$). The PBL moisture convergence alone provides an instability source for the planetary-scale mode (Fig. 5a), and it also accelerates the eastward propagation, making the periodicity fall into the intraseasonal oscillation range for all wavenumbers

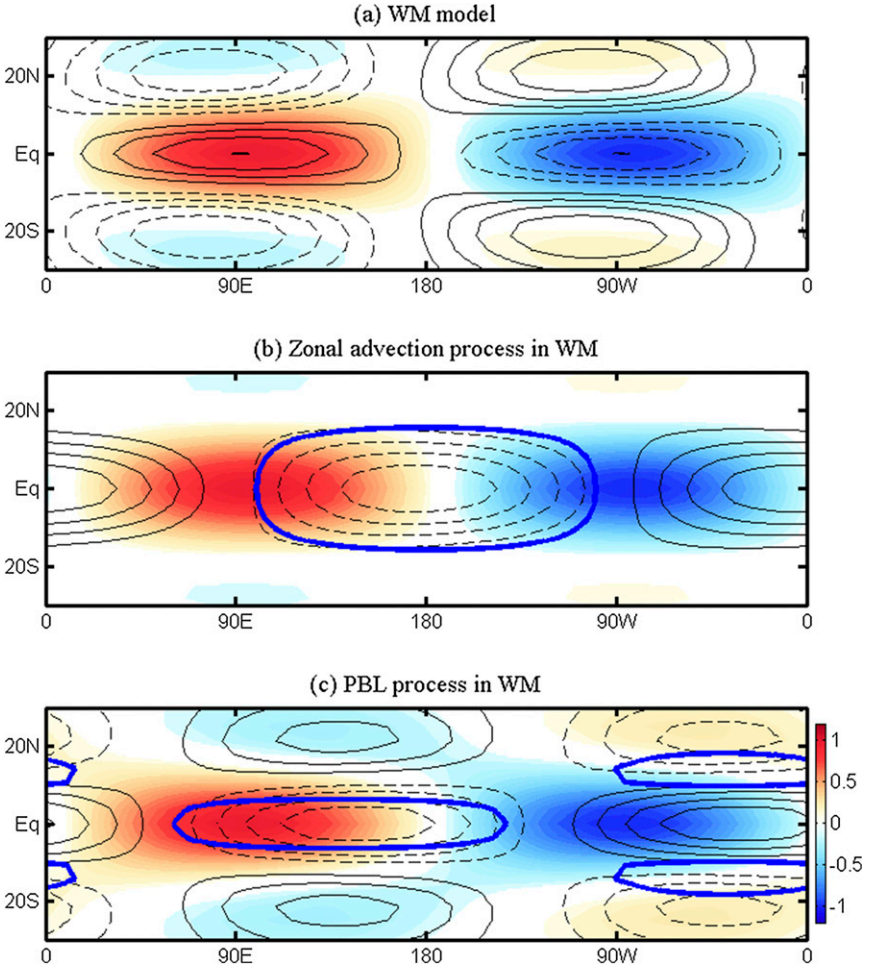

FIG. 4. Horizontal structure changes by different processes. Horizontal structures of normalized precipitation anomalies (shading) and lower-tropospheric pressure anomalies (black contours) for eastward-propagating wavenumber 1 in (a) the original WM model, (b) the WM model with the zonal moisture advection process only, and (c) the WM model with the PBL process only. The contour interval is one-fifth of the maximum amplitude of the anomaly, and the zero contour is not shown. The thick blue contours denote the easterly wind in (b) and upward Ekman pumping in (c), with 0.2 as their amplitudes.

(Fig. 5b). This confirms the result of Liu and Wang (2016). The combined effects of horizontal moisture advection and PBL moisture convergence processes enhance the growth rate of the planetary-scale eastward-propagating mode, resulting in unstable wavenumber 1 through wavenumber 3. Wavenumber 1 has the maximum growth rate, and short waves are damped. Compared to the result from the WM model with the PBL process added, the frequency is increased for all wavenumbers when the moisture advection process is also included. This positive feedback of zonal advection of SMM—namely, increasing the growth rate of planetary-scale waves and accelerating the eastward propagation—can also be shown by two sensitivity experiments with strong and weak zonal advection of SMM in the WM model, which has added both the PBL and horizontal SMM advection processes (Fig. 5). The sensitivity tests on Q and Q_b also show that a stronger growth rate is generated by a warmer SST for all wavenumbers and that planetary-scale waves are slowed down over the warmer SST while short waves are less affected (Liu and Wang 2016).

The PBL moisture convergence has a different impact on the horizontal structure than the SMM advection (Fig. 4c). Rather than having a Kelvin wave–like structure, the PBL moisture convergence couples Kelvin and Rossby waves with precipitation heating and yields a Gill-like anomaly pattern. The equatorial low pressure anomalies, which are in phase with the upward equatorial Ekman pumping, now lead the positive

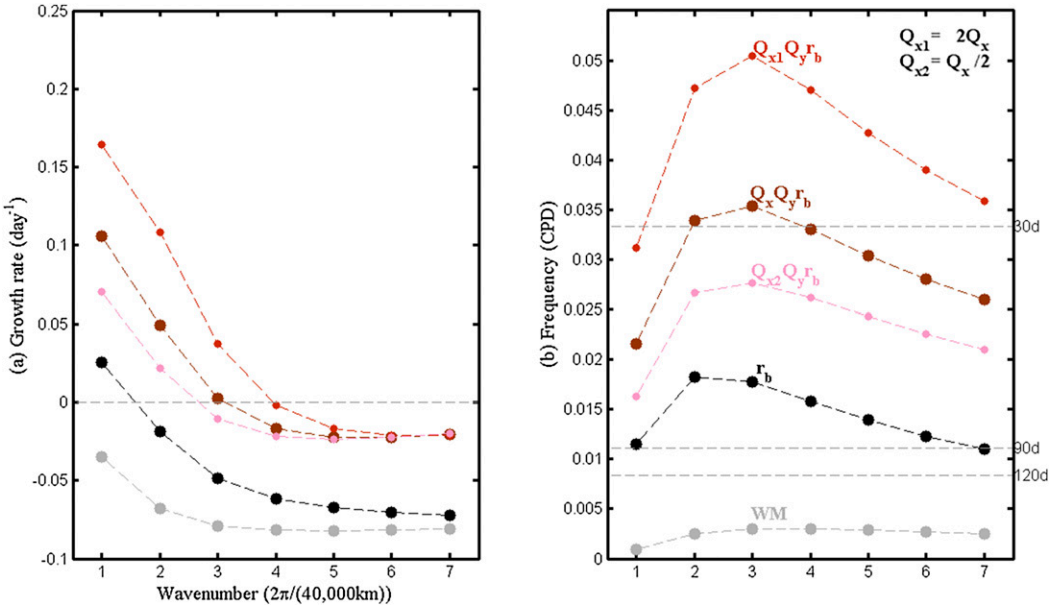

FIG. 5. Roles of PBL and horizontal moisture advection processes. As in Fig. 3, but for the WM model with different processes: PBL alone (black) and both PBL and horizontal moisture advection (brown). Also shown are the results of two sensitivity experiments with strong (red; $Q_{x1} = 2Q_x$) and weak (purple; $Q_{x2} = Q_x/2$) zonal moisture advections in the experiment with both the PBL and horizontal moisture advection processes.

precipitation anomalies. These two features are in good agreement with observations. Therefore, only in the presence of PBL moisture convergence feedback, can the zonal SMM advection mechanism produce realistic horizontal and vertical circulation structures; in addition, it enhances growth rates and makes the eastward propagation faster.

c. *Interpretation of the effects of zonal SMM advection*

How does the zonal SMM advection affect the structure, speed, and instability of eastward propagation? In the WM model, the negative temperature (or positive geopotential) and positive precipitation anomalies are in phase owing to the simplified Betts–Miller parameterization scheme. This relationship is changed by the inclusion of zonal SMM advection. The mean moisture advection provides an additional moisture source moistening the lower troposphere ahead of the precipitation center, which changes the precipitation–geopotential relationship from an in-phase to in-quadrature relationship. In the presence of PBL convergence (Wang and Rui 1990; Liu and Wang 2016), the upward off-equatorial Ekman pumping also enhances the precipitation in the subtropics, which lags its equatorial counterpart. However, the additional moisture advected by the lower-tropospheric easterly wind occurs mainly in the tropical region, which only tends to enhance the precipitation in the equatorial region, resulting in strong equatorially trapped Kelvin wave–like disturbances (Fig. 4b). Since the subtropical perturbation associated with the westward-propagating Rossby component is suppressed and the equatorial precipitation favors the growth of Kelvin waves, the eastward propagation is much accelerated by the zonal SMM advection process.

For the growing modes, positive eddy available potential energy (EAPE) should be generated, which requires positive covariance between perturbation temperature and diabatic heating associated with large-scale precipitation anomalies, or $-\overline{P_r\phi}$ averaged over one wavelength, because on the first baroclinic mode $\phi = -\theta$, where θ is the nondimensional temperature anomaly (Wang and Rui 1990).

Figure 6 compares the EAPE in the WM model with and without the zonal moisture advection and PBL processes. For wavenumber 1 in the WM model (Fig. 6a), strong negative EAPE is generated in the tropics, and weak negative EAPE is in the subtropics. For wavenumber 2, similar negative EAPE is also generated, while positive EAPE is generated near 7°S and 7°N. When the zonal advection of SMM is included (Fig. 6b), similar negative EAPE as that in the WM model can be obtained for wavenumber 2, but positive EAPE, with its maximum value at the equator, is generated for wavenumber 1. In the WM model with the PBL process (Fig. 6c), strong positive EAPE is generated at the equator and in the subtropics for wavenumber 1, while negative EAPE is generated at the equator for wavenumber 2.

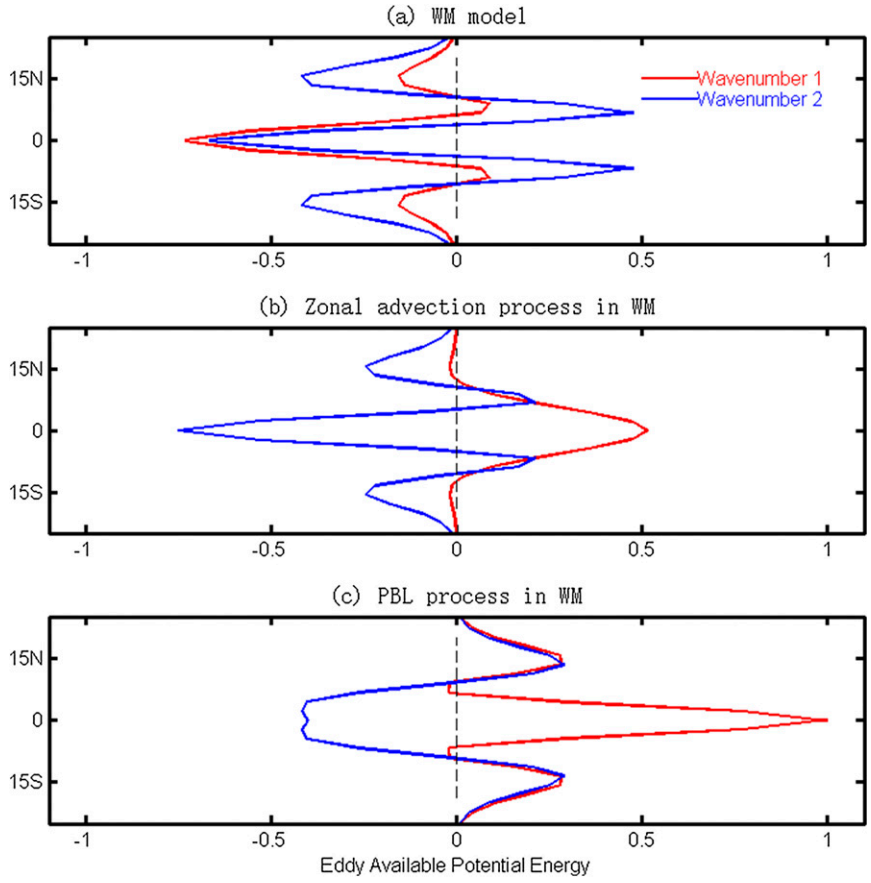

FIG. 6. EAPE changes by different processes. Zonally averaged EAPE of eastward-propagating wavenumber 1 (red) and wavenumber 2 (blue) in (a) the WM model, (b) the WM model with the zonal moisture advection process only, and (c) the WM model with the PBL process only.

In the WM model, the Betts–Miller precipitation scheme is a strong negative feedback, and any disturbances are damped quickly owing to the consumption of convective instability by convection; thus, only negative EAPE is generated. This is in agreement with the result of Liu and Wang (2016). Both the moisture advection and PBL processes provide an instability source for wavenumber 1 and generate positive EAPE. The former is through advecting additional moisture in the equatorial region from the SMM, while the latter is through pumping additional moisture in both equatorial and subtropical regions from the PBL. For shorter waves, the stronger negative feedback of the Betts–Miller scheme dominates, which generates negative EAPE, resulting in damped modes.

d. Sensitivity experiments

The observed SMM has strong zonal variation, in which the eastward gradient exists over the Indo-Pacific warm pool while the westward gradient occurs over the central-eastern Pacific (Fig. 1a). Thus, it is necessary to test how the model evolves under different zonal SMM gradients first.

Figure 7 shows the sensitivity of growth rate and phase speed to different zonal gradients of SMM. When the zonal SMM gradient is positive (negative), the solution for the westward (eastward) propagation has a negative growth rate smaller than $-0.4\,\mathrm{day}^{-1}$ (not shown). When the zonal gradient of SMM is weak (Fig. 7a), both westward and eastward modes are suppressed; when the zonal gradient of SMM is strong, the westward SMM gradient will select the westward propagation as the unstable mode, and the eastward SMM gradient tends to select the eastward propagation. The eastward-propagating (westward propagating) modes have large growth rates when the eastward (westward) SMM gradient is strong. The large eastward (westward) SMM gradient also has strong effect on accelerating the eastward (westward) propagation accordingly (Fig. 7b).

Although precipitation will be damped owing to the consumption of convective instability, the strong zonal advection of SMM does provide additional moisture

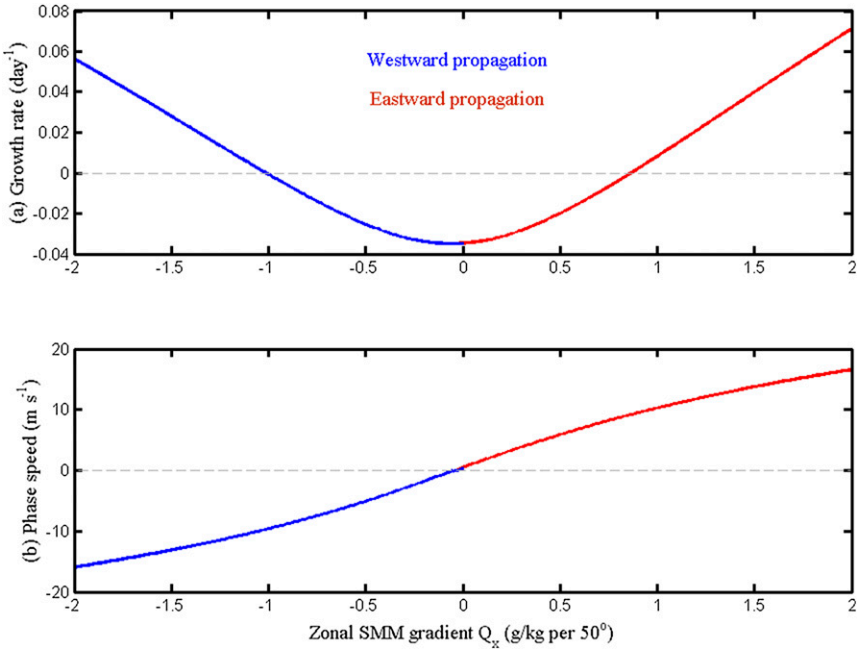

FIG. 7. Sensitivity experiments with different SMM gradients. (a) Growth rate (day^{-1}) and (b) phase speed (m s^{-1}) as a function of SMM gradient for the westward- (blue) and eastward- (red) propagating wavenumber 1 in the WM model with the zonal moisture advection process.

source to the growth of precipitation. The eastward (westward) gradient of SMM will select the eastward (westward) propagation as the growing mode. These results suggest that we should look at the model evolution under a realistic mean state.

4. Realistic mean state

Since the eigenvalue problem cannot deal with a realistic SMM gradient with zonal variation, we need to integrate the model numerically. In these numerical experiments, a realistic SMM gradient with zonal variation is included, and we can simulate longitude-dependent development and propagation. For simplicity, an idealized SST structure mimicking the warm-pool-like SST distribution for the boreal winter is used in the numerical calculation. For simplicity, we use linear heating in the numerical experiments. The nonlinear heating (i.e., the positive-only heating that has been found to select the planetary scale as the most unstable mode; Li and Zhou 2009) is not used here; instead, it will be studied in future.

Figure 8 shows this simple but realistic SST (Fig. 8a), an associated PBL specific-humidity structure (Fig. 8b), and a lower-tropospheric specific-humidity structure (Fig. 8c), which are mainly based on the observation of Fig. 1 and can capture the main characteristics of the observed SMM over the Indo-Pacific region. The lower-tropospheric specific humidity, as well as the SST, is maximum over the warm pool region and decays poleward with a comparable amplitude as the observation (Figs. 8d,e). The experiments under this simple but realistic mean state can demonstrate the roles of PBL moisture convergence and horizontal SMM advection clearly.

In this work, only a theoretical model on the first baroclinic mode is investigated, and many effects of land friction, diurnal cycle, positive-only heating, vertical wind shear, and so forth are not included. In the observation, two SMM peaks occur in Africa and South America (not shown). Dealing with these complicated realistic processes over land and the Maritime Continent is beyond the scope of this work. To isolate the role of SMM advection on the MJO propagation over the Indo-Pacific region, we use this idealized while still realistic mean state.

As shown in Figs. 3 and 5, both the zonal advection of SMM and PBL moisture convergence can provide a positive instability source for the planetary-scale waves. We will study these two processes from the same initial pressure disturbances with a Kelvin wave–like structure of wavenumber 1 while adding one of PBL, advection processes, or both.

Figure 9 shows Hovmöller plots of precipitation at the equator for the calculations with the model including only the PBL moisture convergence, only the horizontal advection of SMM, and both the PBL and

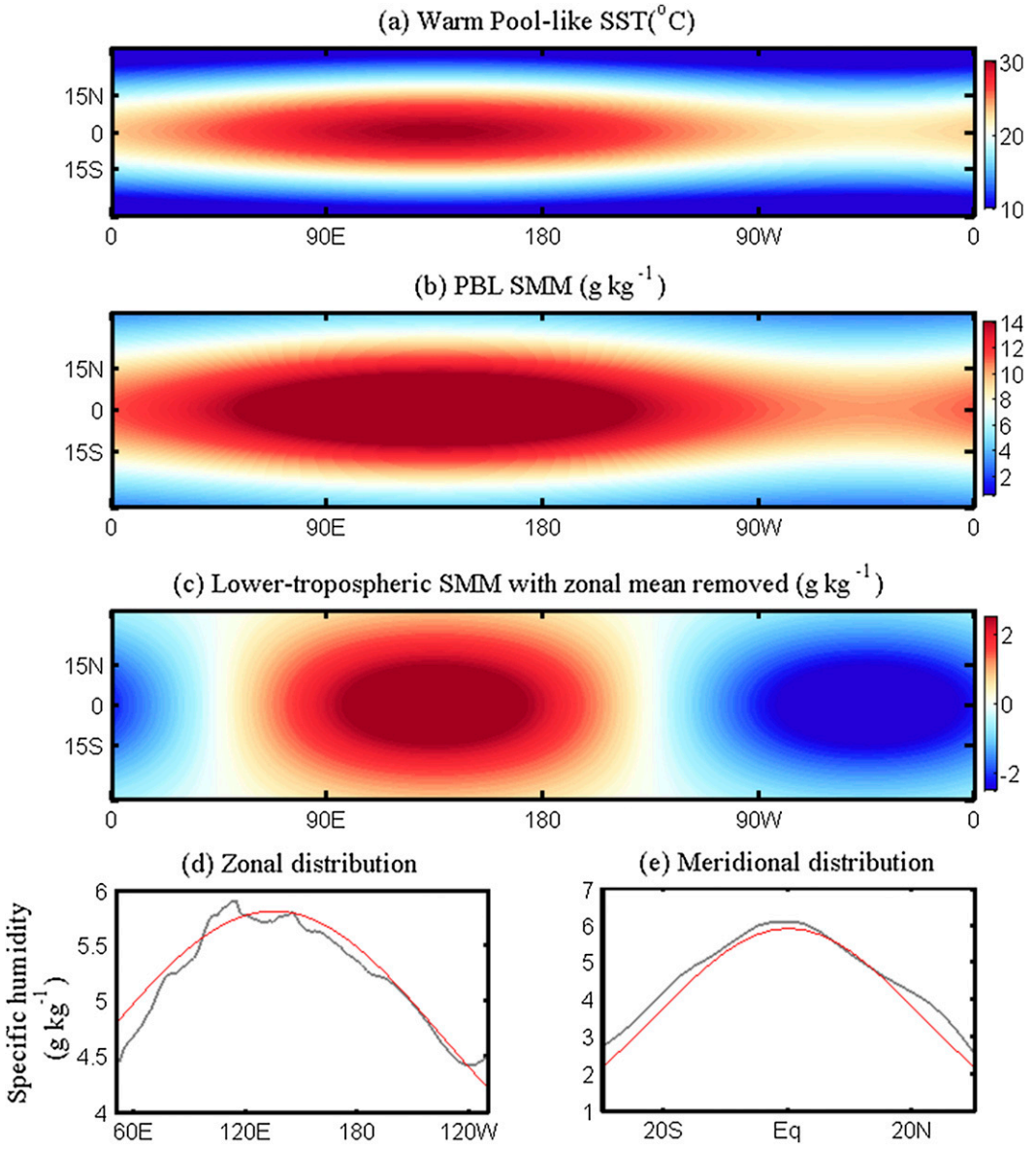

FIG. 8. Warm-pool-like mean state. An idealized warm-pool-like (a) SST (°C) and associated (b) PBL SMM ($g\,kg^{-1}$) and (c) lower-tropospheric SMM ($g\,kg^{-1}$) with the zonal mean removed, which are used in the initial-problem experiments. (d),(e) As in Fig. 1, but the idealized lower-tropospheric SMM is shown by the red line.

moisture advection processes, respectively. Results are shown for a period of 100 days. The PBL moisture convergence only induces eastward-propagating modes, although the precipitation over the cold SST region is weak (Fig. 9a). Since the PBL is mostly wet over the warm pool region (Fig. 8b), the positive feedback of PBL moisture convergence is also maximum there, and so is the lower-tropospheric moisture. The main convection activity occurs over the warm pool region. The horizontal advection of SMM induces both unstable eastward- and westward-propagating modes; over the region with the eastward gradient of SMM, the eastward-propagating mode is enhanced, while over the region where the gradient of SMM is westward, the strong westward-propagating and amplifying mode is simulated (Fig. 9b).

In the solution when both the PBL and advection processes are included (Fig. 9c), the dominant unstable mode is the eastward propagation over the region where the zonal gradient of SMM is eastward, and the eastward propagation speed is close to the observed MJO, $5\,m\,s^{-1}$. In contrast, to the east of the warm pool center (135°E),

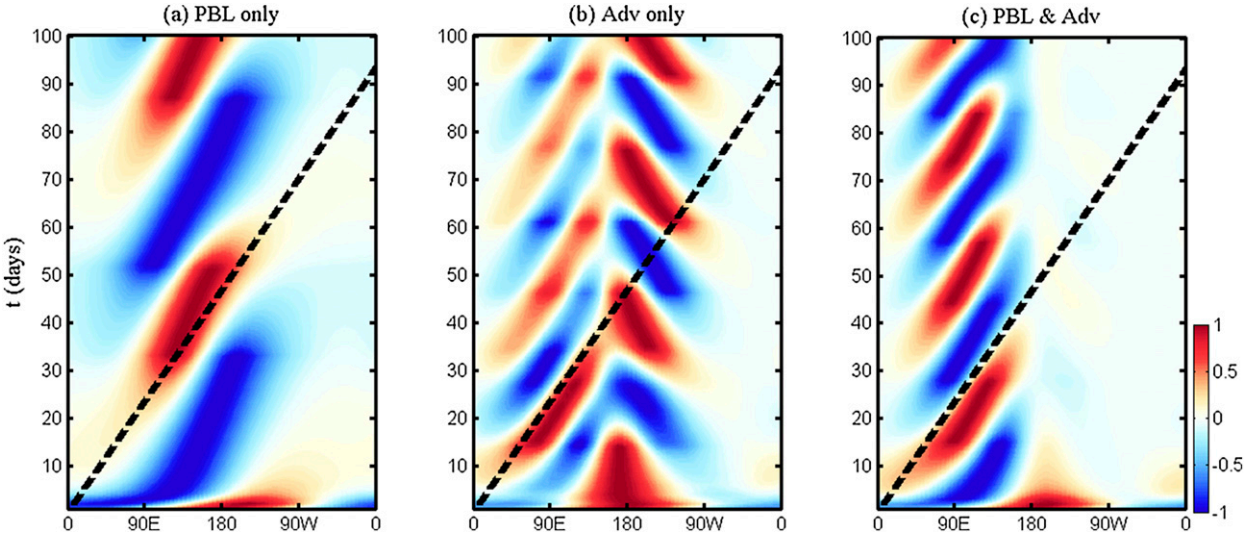

FIG. 9. Zonal propagation changes by different processes. Hovmöller plots of normalized equatorial precipitation in the WM model (a) with the PBL process only, (b) with the horizontal advection of SMM only, and (c) with both the PBL process and horizontal advection of SMM. The initial perturbation has a wavenumber-1 Kelvin wave–like structure. The *x* axis shows longitudinal disturbance, while the *y* axis shows time (days). The dashed line shows the reference speed of 5 m s^{-1}. The equatorial precipitation of each day is normalized.

the westward gradient of SMM favors the growth of westward propagation (Fig. 9b), and the PBL moisture convergence keeps on selecting the eastward propagation (Fig. 9a). These two processes work together and result in weak eastward propagation there.

The horizontal structures of these different propagations are shown in Fig. 10. For the eastward propagation, the Gill-like structure in the simulation with both the PBL and moisture advection processes (Fig. 10c) is mainly caused by the PBL process (Fig. 10a), while the horizontal moisture advection process mainly affects the equatorial region (Fig. 10b). Also seen is that the eastward propagation mode in the moisture advection case decays, while the westward-propagating mode amplifies over the central-eastern Pacific (Fig. 10b). This unrealistic westward propagation is suppressed by the PBL process in the simulation that includes both the PBL and moisture advection processes (Fig. 10c).

The maximum SST is located in 135°E, while the separation between eastward and westward propagation signals is slightly shifted toward 150°E (Fig. 9b). Near the warm pool center with a weak zonal SMM gradient, the convection near the equatorial region is suppressed for both eastward and westward propagations because of negative SMM advection feedback. The wind field is dominated by the equatorial zonal wind for the Kelvin wave–like eastward propagation, while it is also dominated by the subtropical wind for the Rossby wave–like westward propagation. The horizontal SMM advection feedback will enhance the positive precipitation anomalies near the negative precipitation center of the westward propagation; thus, the positive precipitation anomalies will suppress the westward propagation while enhancing the eastward propagation.

It seems that the PBL process alone simulates a more realistic eastward propagation (Figs. 9a and 10a), and the simulation with both the PBL and SMM advection processes presents oscillations that are too frequent and a period that seems too short (Figs. 9c and 10c). Over the Indo-Pacific warm pool region, the eastward propagations in these two simulations have similar phase speeds. The phase speed in the simulation with the PBL process is 3.9 m s^{-1}, and that in the simulation with both the PBL and advection processes is 5.1 m s^{-1}. In the former simulation, the signal will propagate circumglobally, and the period is long. In the latter simulation, the propagation is confined over the Indo-Pacific warm pool region, and the enhanced preceding MJO over the western Pacific will initiate the downstream out-of-phase MJO over the Indian Ocean through moisture advection; thus, the period is short.

In this linear model, the planetary-scale mode has the strongest growth rate; this intrinsic mode will dominate after a long enough period of time. When integrating the same WM model as in Fig. 9c while beginning with small-scale (wavenumber 5), Kelvin wave–like initial pressure disturbances, the strong planetary-scale eastward propagation will dominate after day 20 (not shown). Though the initial disturbances are small scale, the planetary-scale disturbances

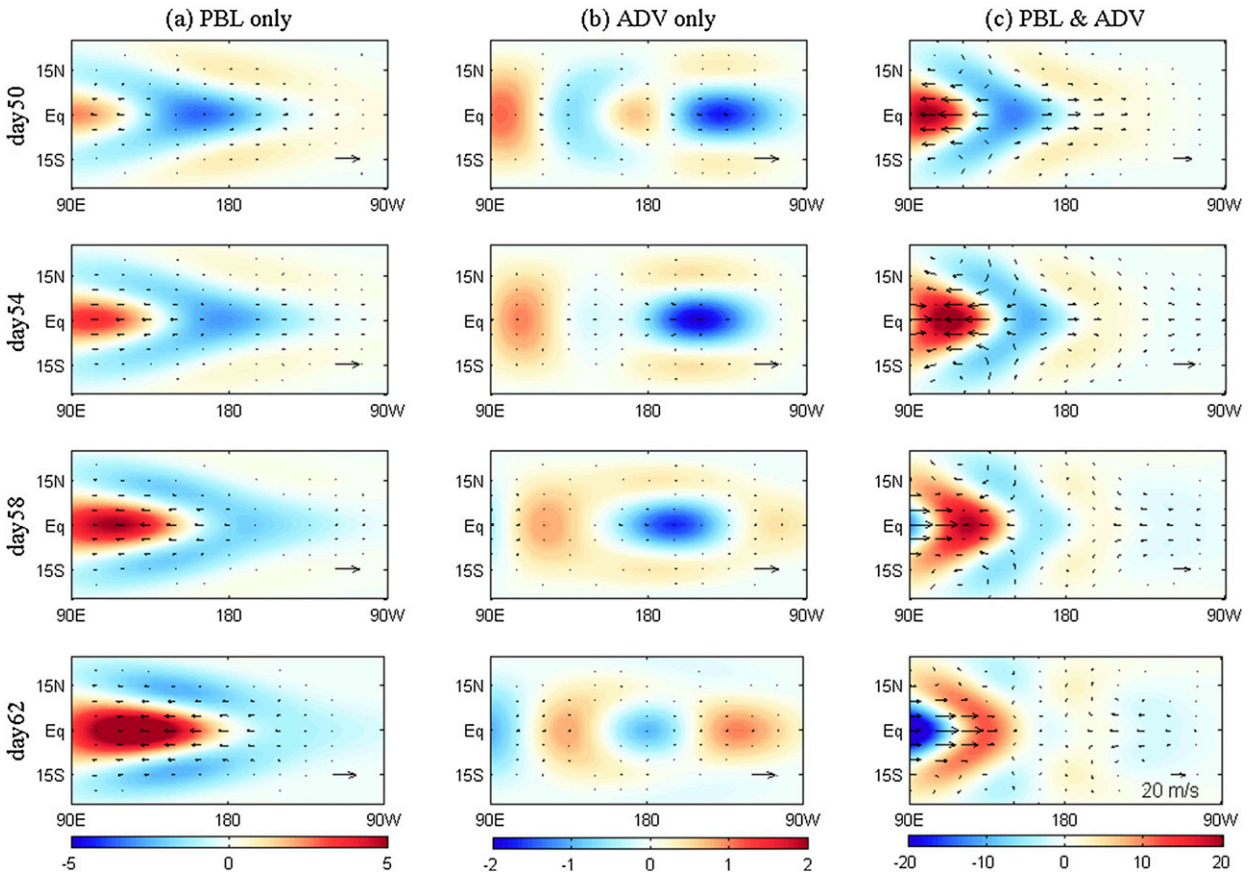

FIG. 10. Horizontal evolution changes by different processes. Shown are precipitation (shading; mm day^{-1}) and lower-level wind (vectors; m s^{-1}) in the WM model (a) with the PBL process only, (b) with the horizontal advection of SMM only, and (c) with both the PBL process and horizontal advection of SMM from day 50 through day 62 by an interval of four days.

grow fast and dominate the eastward propagation over the Indo-Pacific warm pool where the zonal SMM gradient is eastward.

5. Discussion of convection scheme

This work is based on a simple theoretical model for the MJO, and the results are sensitive to different convection schemes. When the precipitation is parameterized by the moisture convergence in both the PBL and lower troposphere, the waves from wavenumber 2 have much higher frequency than the observed MJO (Liu and Wang 2016). By using the MJO skeleton model in which the positive (negative) low-level moisture anomalies are parameterized to create a tendency to enhance (weaken) the envelope of equatorial synoptic-scale wave activity (Majda and Stechmann 2009; Liu and Wang 2012a), our simulations show that the meridional advection of SMM slows down both eastward and westward propagations and creates neutral modes. The zonal advection of SMM with eastward (westward) gradient will disturb the eastward (westward) planetary-scale propagation (not shown).

When using the simplified Betts–Miller scheme in a shallow-water system on the equatorial β plane, the zonal advection of eastward (westward) SMM gradient is also found to provide an instability source for the eastward (westward) propagation (Sukhatme 2014). In Sukhatme's (2014) work, a quick convective adjustment time is used, and only a moist Kelvin wave–like dispersion relation can be obtained. The key to obtaining the MJO-like dispersion relation is using a slow adjustment process (Liu and Wang 2016). A slow adjustment process with a time scale of one day can simulate a reasonable MJO-like dispersion relationship in the ''moisture mode'' (Sobel and Maloney 2012, 2013), in the ''skeleton model'' of the MJO (Majda and Stechmann 2009; Liu and Wang 2012a), and in the WM model (Liu and Wang 2016). When a slow adjustment process is used, quasigeostrophic dynamics in the presence of moisture gradient also give similar results as in the skeleton model: a purely meridional gradient has

the effect of slowing down the dry Rossby waves through a reduction in the "equivalent gradient" of the background potential vorticity. A large-scale unstable moist mode is obtained with the inclusion of a zonal gradient (Monteiro and Sukhatme 2016). We also analyze the observation and find that the precipitation associated with high-frequency Kelvin waves is almost in phase with the lower-tropospheric moisture anomalies, while the precipitation associated with the MJO lags the lower-tropospheric moisture anomalies by 1–3 days (not shown). The former is referred to as a quick convective adjustment process of a few hours, and the latter is referred to as a slow convective adjustment process of one day.

6. Conclusions and remarks

We used a modified version of the MJO theoretical model (Liu and Wang 2016) to explore the role of horizontal advection of SMM in MJO development, propagation, and scale selection. While other processes, such as the PBL moisture convergence, can produce unstable planetary-scale, eastward-propagating disturbances (Fig. 5a), the zonal advection of the eastward SMM gradient can select the planetary-scale eastward-propagating mode as the most unstable mode (Fig. 3a). We believe the SMM advection process is an important mechanism for understanding the MJO formation, as demonstrated by observational analyses (Hsu and Li 2012; Liu et al. 2015) as well as model simulations (Maloney et al. 2010). Over the warm SST of 29.5°C and an eastward SMM gradient of $1.5\,g\,kg^{-1}$ per 50° longitude, which has a similar amplitude with observations over the Indo-Pacific region, the PBL can enhance the growth rate of wavenumber 1 by $0.06\,day^{-1}$ and the SMM advection can induce a growth rate increase of $0.04\,day^{-1}$ compared to the WM model. This result means that the PBL has a somewhat stronger effect on enhancing the eastward-propagating wavenumber 1 than the SMM advection process does.

The SMM advection mechanism alone produces an unrealistic Kelvin wave–like structure (Figs. 4b and 10b) and prevailing westward propagation in the central-eastern Pacific where the SMM decreases eastward (Fig. 9b), both of which disagree with observations. These caveats, however, can be remitted if the PBL moisture convergence is included (Fig. 10c); the model then produces a convectively coupled Kelvin–Rossby wave structure and suppresses the unrealistic, growing westward-propagating mode.

In the linear regime, the growth rate and phase speed are sensitive to the gradient of SMM (Fig. 7). The fast development and slow eastward propagation of the MJO were simulated over the Indian Ocean where the SMM gradient is eastward, while the westward SMM gradient would damp the eastward-propagating MJO in the central-eastern Pacific (Fig. 9). All these results suggest that, although the coupling between the moisture convergence of frictional PBL and free-tropospheric counterpart is important for MJO simulation in GCMs (Jiang et al. 2015), the model's mean state, especially the SMM, can also play a role in MJO simulation in these models (Kim et al. 2011; Benedict et al. 2014).

Acknowledgments. This work was supported by the China National 973 Project (2015CB453200), the National Natural Science Foundation of China (41420104002), the Natural Science Foundation of Jiangsu Province (BK20150907 and BK20150062), Jiangsu Specially Appointed Professor (R2015T13), the Priority Academic Program Development of Jiangsu Higher Education Institutions (PAPD), and Jiangsu Shuang-Chuang Team (R2014SCT01). BW acknowledges support from the U.S. National Science Foundation (climate dynamics division Award AGS-1540783), NOAA ESS (Award NA13OAR4310167), and the Global Research Laboratory (GRL) Program of the National Research Foundation of Korea (Grant 2011-0021927).

REFERENCES

Andersen, J. A., and Z. Kuang, 2012: Moist static energy budget of MJO-like disturbances in the atmosphere of a zonally symmetric aquaplanet. *J. Climate*, **25**, 2782–2804, doi:10.1175/JCLI-D-11-00168.1.

Benedict, J. J., E. D. Maloney, A. H. Sobel, and D. M. Frierson, 2014: Gross moist stability and MJO simulation skill in three full-physics GCMs. *J. Atmos. Sci.*, **71**, 3327–3349, doi:10.1175/JAS-D-13-0240.1.

Betts, A., 1986: A new convective adjustment scheme. Part I: Observational and theoretical basis. *Quart. J. Roy. Meteor. Soc.*, **112**, 677–691, doi:10.1002/qj.49711247307.

——, and M. Miller, 1986: A new convective adjustment scheme. Part II: Single column tests using GATE wave, BOMEX, ATEX and arctic air-mass data sets. *Quart. J. Roy. Meteor. Soc.*, **112**, 693–709, doi:10.1002/qj.49711247308.

Bretherton, C. S., M. E. Peters, and L. E. Back, 2004: Relationships between water vapor path and precipitation over the tropical oceans. *J. Climate*, **17**, 1517–1528, doi:10.1175/1520-0442(2004)017<1517:RBWVPA>2.0.CO;2.

Emanuel, K. A., 1987: An air–sea interaction model of intraseasonal oscillations in the tropics. *J. Atmos. Sci.*, **44**, 2324–2340, doi:10.1175/1520-0469(1987)044<2324:AASIMO>2.0.CO;2.

Frierson, D. M., A. J. Majda, and O. M. Pauluis, 2004: Large scale dynamics of precipitation fronts in the tropical atmosphere: A novel relaxation limit. *Commun. Math. Sci.*, **2**, 591–626, doi:10.4310/CMS.2004.v2.n4.a3.

Fuchs, Z., and D. J. Raymond, 2005: Large-scale modes in a rotating atmosphere with radiative–convective instability and WISHE. *J. Atmos. Sci.*, **62**, 4084–4094, doi:10.1175/JAS3582.1.

Grabowski, W. W., and M. Moncrieff, 2004: Moisture–convection feedback in the tropics. *Quart. J. Roy. Meteor. Soc.*, **130**, 3081–3104, doi:10.1256/qj.03.135.

Hendon, H. H., and M. L. Salby, 1994: The life cycle of the Madden–Julian oscillation. *J. Atmos. Sci.*, **51**, 2225–2237, doi:10.1175/1520-0469(1994)051<2225:TLCOTM>2.0.CO;2.

Hsu, P.-C., and T. Li, 2012: Role of the boundary layer moisture asymmetry in causing the eastward propagation of the Madden–Julian oscillation. *J. Climate*, **25**, 4914–4931, doi:10.1175/JCLI-D-11-00310.1.

Hu, Q., and D. A. Randall, 1994: Low-frequency oscillations in radiative–convective systems. *J. Atmos. Sci.*, **51**, 1089–1099, doi:10.1175/1520-0469(1994)051<1089:LFOIRC>2.0.CO;2.

Jiang, X., and Coauthors, 2015: Vertical structure and physical processes of the Madden–Julian oscillation: Exploring key model physics in climate simulations. *J. Geophys. Res. Atmos.*, **120**, 4718–4748, doi:10.1002/2014JD022375.

Kalnay, E., and Coauthors, 1996: The NCEP/NCAR 40-Year Reanalysis Project. *Bull. Amer. Meteor. Soc.*, **77**, 437–471, doi:10.1175/1520-0477(1996)077<0437:TNYRP>2.0.CO;2.

Kanamitsu, M., W. Ebisuzaki, J. Woollen, S.-K. Yang, J. Hnilo, M. Fiorino, and G. Potter, 2002: NCEP–DOE AMIP-II Reanalysis (R-2). *Bull. Amer. Meteor. Soc.*, **83**, 1631–1643, doi:10.1175/BAMS-83-11-1631.

Kang, I.-S., F. Liu, M.-S. Ahn, Y.-M. Yang, and B. Wang, 2013: The role of SST structure in convectively coupled Kelvin–Rossby waves and its implications for MJO formation. *J. Climate*, **26**, 5915–5930, doi:10.1175/JCLI-D-12-00303.1.

Kiladis, G. N., K. H. Straub, and P. T. Haertel, 2005: Zonal and vertical structure of the Madden–Julian oscillation. *J. Atmos. Sci.*, **62**, 2790–2809, doi:10.1175/JAS3520.1.

Kim, D., A. H. Sobel, E. D. Maloney, D. M. Frierson, and I.-S. Kang, 2011: A systematic relationship between intraseasonal variability and mean state bias in AGCM simulations. *J. Climate*, **24**, 5506–5520, doi:10.1175/2011JCLI4177.1.

Kiranmayi, L., and E. D. Maloney, 2011: Intraseasonal moist static energy budget in reanalysis data. *J. Geophys. Res.*, **116**, D21117, doi:10.1029/2011JD016031.

Knutson, T. R., and K. M. Weickmann, 1987: 30–60 day atmospheric oscillations: Composite life cycles of convection and circulation anomalies. *Mon. Wea. Rev.*, **115**, 1407–1436, doi:10.1175/1520-0493(1987)115<1407:DAOCLC>2.0.CO;2.

Kuang, Z., 2011: The wavelength dependence of the gross moist stability and the scale selection in the instability of column-integrated moist static energy. *J. Atmos. Sci.*, **68**, 61–74, doi:10.1175/2010JAS3591.1.

Lau, K., and L. Peng, 1987: Origin of low-frequency (intraseasonal) oscillations in the tropical atmosphere. Part I: Basic theory. *J. Atmos. Sci.*, **44**, 950–972, doi:10.1175/1520-0469(1987)044<0950:OOLFOI>2.0.CO;2.

Li, T., and C. Zhou, 2009: Planetary scale selection of the Madden–Julian oscillation. *J. Atmos. Sci.*, **66**, 2429–2443, doi:10.1175/2009JAS2968.1.

Liebmann, B., and C. A. Smith, 1996: Description of a complete (interpolated) outgoing longwave radiation dataset. *Bull. Amer. Meteor. Soc.*, **77**, 1275–1277.

Liu, F., and B. Wang, 2012a: A frictional skeleton model for the Madden–Julian oscillation. *J. Atmos. Sci.*, **69**, 2749–2758, doi:10.1175/JAS-D-12-020.1.

——, and ——, 2012b: A model for the interaction between 2-day waves and moist Kelvin waves. *J. Atmos. Sci.*, **69**, 611–625, doi:10.1175/JAS-D-11-0116.1.

——, and ——, 2013: Impacts of upscale heat and momentum transfer by moist Kelvin waves on the Madden–Julian oscillation: A theoretical model study. *Climate Dyn.*, **40**, 213–224, doi:10.1007/s00382-011-1281-0.

——, and ——, 2016: Effects of moisture feedback in a frictional coupled Kelvin–Rossby wave model and implication in the Madden–Julian oscillation dynamics. *Climate Dyn.*, doi:10.1007/s00382-016-3090-y, in press.

——, L. Zhou, J. Ling, X. Fu, and G. Huang, 2015: Relationship between SST anomalies and the intensity of intraseasonal variability. *Theor. Appl. Climatol.*, **124**, 847–854, doi:10.1007/s00704-015-1458-2.

Madden, R. A., and P. R. Julian, 1971: Detection of a 40–50 day oscillation in the zonal wind in the tropical Pacific. *J. Atmos. Sci.*, **28**, 702–708, doi:10.1175/1520-0469(1971)028<0702:DOADOI>2.0.CO;2.

——, and ——, 1972: Description of global-scale circulation cells in the tropics with a 40–50 day period. *J. Atmos. Sci.*, **29**, 1109–1123, doi:10.1175/1520-0469(1972)029<1109:DOGSCC>2.0.CO;2.

——, and ——, 1994: Observations of the 40–50-day tropical oscillation—A review. *Mon. Wea. Rev.*, **122**, 814–837, doi:10.1175/1520-0493(1994)122<0814:OOTDTO>2.0.CO;2.

Majda, A. J., and J. A. Biello, 2004: A multiscale model for tropical intraseasonal oscillations. *Proc. Natl. Acad. Sci. USA*, **101**, 4736–4741, doi:10.1073/pnas.0401034101.

——, and S. N. Stechmann, 2009: The skeleton of tropical intraseasonal oscillations. *Proc. Natl. Acad. Sci. USA*, **106**, 8417–8422, doi:10.1073/pnas.0903367106.

——, and ——, 2011: Nonlinear dynamics and regional variations in the MJO skeleton. *J. Atmos. Sci.*, **68**, 3053–3071, doi:10.1175/JAS-D-11-053.1.

Maloney, E. D., 2009: The moist static energy budget of a composite tropical intraseasonal oscillation in a climate model. *J. Climate*, **22**, 711–729, doi:10.1175/2008JCLI2542.1.

——, and D. L. Hartmann, 1998: Frictional moisture convergence in a composite life cycle of the Madden–Julian oscillation. *J. Climate*, **11**, 2387–2403, doi:10.1175/1520-0442(1998)011<2387:FMCIAC>2.0.CO;2.

——, A. H. Sobel, and W. M. Hannah, 2010: Intraseasonal variability in an aquaplanet general circulation model. *J. Adv. Model. Earth Syst.*, **2**, 1–14, doi:10.3894/JAMES.2010.2.5.

Monteiro, J. M., and J. Sukhatme, 2016: Quasi-geostrophic dynamics in the presence of moisture gradients. *Quart. J. Roy. Meteor. Soc.*, **142**, 187–195, doi:10.1002/qj.2644.

Neelin, J. D., and J.-Y. Yu, 1994: Modes of tropical variability under convective adjustment and the Madden–Julian oscillation. Part I: Analytical theory. *J. Atmos. Sci.*, **51**, 1876–1894, doi:10.1175/1520-0469(1994)051<1876:MOTVUC>2.0.CO;2.

——, I. M. Held, and K. H. Cook, 1987: Evaporation–wind feedback and low-frequency variability in the tropical atmosphere. *J. Atmos. Sci.*, **44**, 2341–2348, doi:10.1175/1520-0469(1987)044<2341:EWFALF>2.0.CO;2.

Raymond, D. J., 2001: A new model of the Madden–Julian oscillation. *J. Atmos. Sci.*, **58**, 2807–2819, doi:10.1175/1520-0469(2001)058<2807:ANMOTM>2.0.CO;2.

——, and Ž. Fuchs, 2009: Moisture modes and the Madden–Julian oscillation. *J. Climate*, **22**, 3031–3046, doi:10.1175/2008JCLI2739.1.

Sobel, A., and E. Maloney, 2012: An idealized semi-empirical framework for modeling the Madden–Julian oscillation. *J. Atmos. Sci.*, **69**, 1691–1705, doi:10.1175/JAS-D-11-0118.1.

——, and ——, 2013: Moisture modes and the eastward propagation of the MJO. *J. Atmos. Sci.*, **70**, 187–192, doi:10.1175/JAS-D-12-0189.1.

——, J. Nilsson, and L. M. Polvani, 2001: The weak temperature gradient approximation and balanced tropical moisture waves. *J. Atmos. Sci.*, **58**, 3650–3665, doi:10.1175/1520-0469(2001)058<3650:TWTGAA>2.0.CO;2.

——, S. Wang, and D. Kim, 2014: Moist static energy budget of the MJO during DYNAMO. *J. Atmos. Sci.*, **71**, 4276–4291, doi:10.1175/JAS-D-14-0052.1.

Sukhatme, J., 2014: Low-frequency modes in an equatorial shallow-water model with moisture gradients. *Quart. J. Roy. Meteor. Soc.*, **140**, 1838–1846, doi:10.1002/qj.2264.

Wang, B., 1988a: Dynamics of tropical low-frequency waves: An analysis of the moist Kelvin wave. *J. Atmos. Sci.*, **45**, 2051–2065, doi:10.1175/1520-0469(1988)045<2051:DOTLFW>2.0.CO;2.

——, 1988b: Comments on "An air–sea interaction model of intraseasonal oscillation in the tropics." *J. Atmos. Sci.*, **45**, 3521–3525, doi:10.1175/1520-0469(1988)045<3521:COAIMO>2.0.CO;2.

——, and H. Rui, 1990: Dynamics of the coupled moist Kelvin–Rossby wave on an equatorial β-plane. *J. Atmos. Sci.*, **47**, 397–413, doi:10.1175/1520-0469(1990)047<0397:DOTCMK>2.0.CO;2.

——, and T. Li, 1994: Convective interaction with boundary-layer dynamics in the development of a tropical intraseasonal system. *J. Atmos. Sci.*, **51**, 1386–1400, doi:10.1175/1520-0469(1994)051<1386:CIWBLD>2.0.CO;2.

——, and F. Liu, 2011: A model for scale interaction in the Madden–Julian oscillation. *J. Atmos. Sci.*, **68**, 2524–2536, doi:10.1175/2011JAS3660.1.

Wang, S., A. H. Sobel, and Z. Kuang, 2013: Cloud-resolving simulation of TOGA-COARE using parameterized large-scale dynamics. *J. Geophys. Res. Atmos.*, **118**, 6290–6301, doi:10.1002/jgrd.50510.

Wheeler, M. C., and H. H. Hendon, 2004: An all-season real-time multivariate MJO index: Development of an index for monitoring and prediction. *Mon. Wea. Rev.*, **132**, 1917–1932, doi:10.1175/1520-0493(2004)132<1917:AARMMI>2.0.CO;2.

Woolnough, S., J. Slingo, and B. Hoskins, 2001: The organization of tropical convection by intraseasonal sea surface temperature anomalies. *Quart. J. Roy. Meteor. Soc.*, **127**, 887–907, doi:10.1002/qj.49712757310.

Zhang, C., 2005: Madden–Julian oscillation. *Rev. Geophys.*, **43**, RG2003, doi:10.1029/2004RG000158.

Zhao, C., T. Li, and T. Zhou, 2013: Precursor signals and processes associated with MJO initiation over the tropical Indian Ocean. *J. Climate*, **26**, 291–307, doi:10.1175/JCLI-D-12-00113.1.